Chemical Science

ROYAL SOCIETY OF CHEMISTRY

EDGE ARTICLE

View Article Online
View Journal | View Issue

Cite this: *Chem. Sci.*, 2025, **16**, 18278

All publication charges for this article have been paid for by the Royal Society of Chemistry

Tuning the surface chemistry of NHC-protected Au_{13} nanoclusters *via* a robust amide coupling procedure

Andrew L. D. M. Laluk, [ab] Dennis A. Buschmann, [bd] Shinjiro Takano, [bd] Angus I. Sullivan, [ab] Parimah Aminfar, [ab] Kevin Stamplecoskie, *[ab] Tatsuya Tsukuda *[bd] and Cathleen M. Crudden *[abc]

There is significant potential use for gold nanoclusters in biomedicine owing to their favorable biological and optical properties. To access this potential, there is a need for methods to alter the ligand scaffold of gold nanoclusters to tune their biological properties. Surface modifications to the ligands must occur with molecular precision to generate monodisperse products for the accurate determination of structure activity relationships and eventual translation to clinical practice. Herein, we describe methods for molecularly precise surface modifications to Au_{13} nanoclusters *via* amide couplings to –COOH functionalities and their stability to conditions necessary for the removal of protecting groups used in amide coupling chemistry. These clusters were found to be highly stable to basic conditions for the removal of base-labile -Fmoc and -OMe groups but less stable to acidic conditions for the removal of acid-labile -Boc and -O^{t}Bu groups. The ligand shell and Au_{13} core of such clusters were found to be preserved following modifications to the ligand shell allowing the solubility and biological properties of the cluster to be altered independently of their optical properties. The nature of the protecting ligand was found be instrumental for cluster stability to enable the use of the harsh conditions necessary to yield monodisperse products.

Received 22nd April 2025
Accepted 31st July 2025

DOI: 10.1039/d5sc02951a

rsc.li/chemical-science

Introduction

Gold nanoclusters (AuNCs) are interesting nanomaterials with high promise for biomedical applications due to their favorable biocompatibility, ability to be chemically modified, and tunable optical properties.[1–4] The atomic precision of these materials arguably provides the best opportunity for the development of robust structure–activity relationships and optimization of properties. Key properties for any biomedical application include stability, water solubility, bio-compatibility, photoluminescence intensity, and emission wavelength.[5,6]

The ligands employed to support AuNCs are critical for their stability, and provide opportunities to control structure, tune physical properties and append biologically relevant ligands.[3,7–9] Thiolates,[8,10] alkynyls,[11,12] phosphines[13] and more recently, N-heterocyclic carbenes (NHCs)[14,15] are the main ligands employed to stabilize AuNCs. L-type ligands such as phosphines and NHCs typically cause a reduction of the HOMO–LUMO gap of the nanocluster, shifting emission wavelengths to the near infrared region where tissue penetration is greater.[16] However, photoluminescence quantum yields (PLQYs) of known NHC-stabilized clusters are reported to be considerably higher, reaching 62% for superatom-type clusters and 30% for coordination clusters.[16,17]

Despite a growing abundance of NHC-protected AuNCs with various gold core sizes and ligand structures,[8,10,18–22] there are few reports of functionalization of the ligand shell to introduce tumor-targeting agents or to optimize physical properties.[6,23,24] Post-synthetic functionalization of AuNCs has been achieved,[25,26] but is often complicated by incomplete reactions on the ligand layers[27–32] and instability under reaction conditions can lead to decomposition, aggregation, or structural rearrangement of the gold core under conditions required for their functionalization.[33–35] Most importantly, there is a lack of knowledge of the effect of ligand structure on the efficiency of these bioconjugation reactions.

Considering these issues and our interest in the use of NHC-stabilized AuNCs for biological applications, we set out to develop conditions for complete bioconjugation reactions at the ligand without disrupting the gold core. Herein we describe the use of amide coupling reactions for bioconjugation on NHC-

[a]*Department of Chemistry, Queen's University, Chernoff Hall, Kingston, Ontario K7L 3N6, Canada. E-mail: cruddenc@queensu.ca; kevin.stamplecoskie@queensu.ca*
[b]*Carbon to Metal Coating Institute, Queen's University, Kingston, Ontario, K7L 3N6, Canada*
[c]*Institute of Transformative Bio-Molecules (WPI-ITbM), Nagoya University, Chikusa, Nagoya 464-8602, Japan*
[d]*Department of Chemistry, Graduate School of Science, The University of Tokyo, 7-3-1 Hongo, Bunkyo-ku, Tokyo, 113-0033, Japan. E-mail: tsukuda@chem.s.u-tokyo.ac.jp*

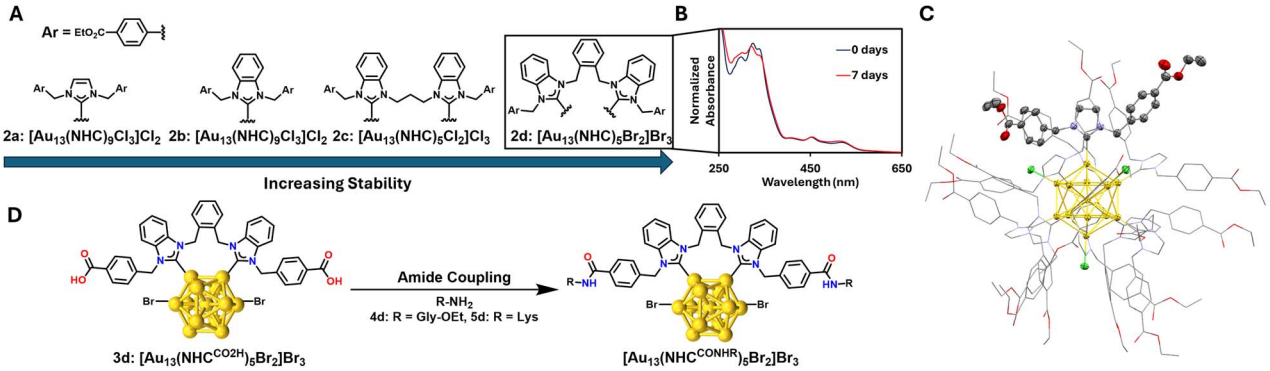

Fig. 1 (A) Ligand dependent stability trends of $-CO_2Et$ functionalized Au_{13} clusters (**2a–d**). (B) Absorption spectra of **2d** taken before and after heating at 90 °C for 4 days in 1 : 1 EtOH : H_2O with 30 eq. KOH followed by 3 days in H_2O with 30 eq. KOH, with absorbances normalized at 453 nm. (C) Coordination structure of **2a[PF$_6$]$_2$**, only one NHC ligand is highlighted for clarity (grey = carbon; yellow = gold; red = oxygen; blue = nitrogen; green = chlorine). (D) Amide coupling procedure for bioconjugation of amino acids to **3d**.

stabilized AuNCs (Fig. 1C). The stability of the ligand shell is critical to enable reaction of all 10 NHC-appended carboxylic acids without decomposition of the AuNC. We also describe the key structural features of the NHC ligands that enable them to survive these sometimes harsh conditions (Fig. 1A and B) and explore the effect of post-synthetic modifications to the NHC ligands on the photophysical properties of the AuNCs.

Results and discussion

Synthesis and characterization of Au_{13}^{CO2Et} nanoclusters

We began by investigating the effect of the NHC structure on the resulting Au_{13} clusters. Monodentate and bidentate ligands were compared, as was the impact of benzannulation and the nature of the linking groups for bidentate ligands. Benzyl groups were employed as wingtip groups and as the point of introduction of ester units for bioconjugation efforts. Details of the ligand synthesis can be found in the SI.

After the desired ligands were prepared, conversion into their respective molecular gold complexes (NHC^{CO2Et})AuX (**1a–b**) and (NHC^{CO2Et})$_2$(Au_2X_2) (**1c–d**) was achieved by stirring in acetone at 60 °C in the presence of K_2CO_3 and $(CH_3)_2SAuCl$. Reduction of **1a–d** with $NaBH_4$, followed by treatment with HCl or HBr,[36] and purification by column chromatography gave the desired ethyl ester-functionalized Au_{13} nanoclusters **2a–d** (Fig. 1A).

During this procedure, the monodentate imidazolylidene NHC-supported cluster [Au_{13}($^{Im}NHC^{CO2Et}$)$_9Cl_3$]Cl_2 (**2a**) stood out as the least stable, since a notable degree of decomposition was observed during chromatographic purification. However, the large difference in solubility between the cluster and molecular NHC–Au–X complexes enabled purification by repeated washing with MeOH. Cluster **2b** is identical except for the presence of benzannulation on the NHC, this small change provided higher stability to the cluster, with only small amounts of decomposition observed during chromatography. Previous crystallographic studies have shown that CH–π and π–π interactions exist between the benzyl wingtips and the benzannulated NHC backbone of similar monotopic NHC protected clusters.[37] These stabilizing interactions afforded by benzannulation of the NHC ligands in **2b** likely contribute to the increased stability of benzannulated clusters relative to simple imidazolylidene derivatives (**2a**). This illustrates that non-covalent interactions need to be taken into account along with the strength of the NHC–Au bond. Since the introduction of benzannulation on the NHC ligand affords increased stability to the cluster, ditopic ligands with benzannulated NHCs were prepared next.

Clusters prepared from ditopic NHC (diNHC) ligands (**2c–d**) with the general formula [Au_{13}($^{Bzim}NHC^{CO2Et}$)$_5X_2$]X_3 did show significantly greater stability compared with **2a–b**, with no signs of decomposition during chromatography. The stability of the diNHC ligated clusters is similar to those previously reported, indicating that cluster stability is largely unchanged by introducing ester substituents at the para position of the benzyl wingtip groups.[37,38]

Single-crystals of the monotopic clusters [Au_{13}($^{Im}NHC^{CO2Et}$)$_9Cl_3$][PF_6]$_2$ (**2a[PF$_6$]$_2$**, space group $P2_1/n$) were obtained by layering dichloromethane/methanol solutions with *n*-hexane (Fig. 1D). The bond lengths between the surface gold atoms (Au_s) and the central gold atom (Au_c) were in the range of 2.7336(10)–2.7859(11) Å with an average bond length of 2.7585 Å. The known cluster lacking the CO_2Et group, [Au_{13}($Bzim^{Bn}$)$_9$-Cl_3][PF_6]$_2$ (**(Z)**, space group $P\bar{1}$),[37] was previously characterized by single-crystal X-ray crystallography, with slightly longer Au_s–Au_c bond lengths (2.7308(8)–2.8049(8) Å, avg. = 2.7681 Å). These marginal differences in Au–Au bond lengths may be attributed to the increased steric hindrance of the ligand system in **2a** due to the additional COOEt groups resulting in different crystal packing (Table 1).

Table 1 Au–Au Bond Lengths of the Au_{13} Core

	Average bond length (Å)	
Cluster	Au_s–Au_c	Au_s–Au_s
2a	2.760 ± 0.015	2.902 ± 0.038
Z	2.768 ± 0.023	2.911 ± 0.037

Saponification of Au_{13}^{CO2Et} Nanoclusters (2a–d)

To obtain the free carboxylic acid functionalities necessary for amide couplings, clusters **2a–d** were subjected to saponification conditions. Cluster **2a** decomposed completely after treatment with 25 eq. KOH in a 1 : 1 EtOH/H_2O mixture at ambient temperature for 4 h, consistent with the lower stability of this cluster observed during purification. In contrast, saponification, although incomplete, was observed for the monodentate benzimidazole variant (**2b**) and the propyl linked ditopic cluster (**2c**) under the same conditions with gradual decomposition. ESI-MS revealed that while the Au_{13} core remained intact, the reaction solution featured a mixture of Au_{13} clusters with differently saponified ligand shells (Fig. S18 and S19). Due to the similar surface chemistry and size of the clusters in the crude product, such mixtures could not be separated to generate a single product, though a separation of the cluster species from smaller Au–NHC complexes was accomplished *via* ultrafiltration using a 3 kDa molecular weight cutoff filter by spinning at 3500 rpm for 60 minutes at a flux of 20 mL per hour and repeating this process until the filtrate was colourless. Further attempts to achieve complete saponification of clusters **2a–c** by increasing the temperature of the solution, reaction time, or equivalents of base resulted in the decomposition of the Au_{13} core prior to complete saponification of the ligands.

Next, we turned to cluster **2d** as one of the most stable clusters in this series. Mild saponification conditions at room temperature with few equivalents of base resulted in incomplete saponification of **2d**. However, cluster **2d** could be subjected to harshly basic conditions at high temperatures without decomposition as shown by UV-vis absorption spectra taken before and after heating at 90 °C for 4 days in 1 : 1 EtOH : H_2O with 30 eq. KOH followed by 3 days in H_2O with 30 eq. KOH indicate minimal decomposition of the Au_{13} core (Fig. 1B). The higher stability of cluster **2d** under harshly basic conditions allowed it to survive conditions necessary to induce complete saponification of all 10 surface ester functionalities (Fig. 2D). Reaction times were reduced from 1 week to 2 hours using DMSO instead of EtOH as a co-solvent to solubilize **2d** in aqueous solutions (Fig. 2A and D). A small amount of decomposition was observed, generating some NHC–Au-X complex impurities, but these were easily removed *via* size exclusion chromatography (see SI for details) to generate **3d** in high purity and yields (84%). ^{1}H NMR spectra of **3d** showed the successful removal of the characteristic signals centered at 4.1 ppm (–OCH_2) and 1.3 ppm (–CH_3) of the ethyl ester present in the ^{1}H NMR of **2d**, and the presence of a broad singlet at 12.6 ppm associated with the new –CO_2H functionality (Fig. 2B and C). Cluster **3d** was observed to be soluble in aqueous solutions at pH > 4, at which the carboxylic acids are deprotonated.

The high thermal stability of the diNHC-protected cluster **2d** compared to monotopic NHC-protected clusters **2a** and **2b** was expected based on previous reports of related NHC-protected Au_{13} clusters.[37,38] However, a comparison of the propyl-linked

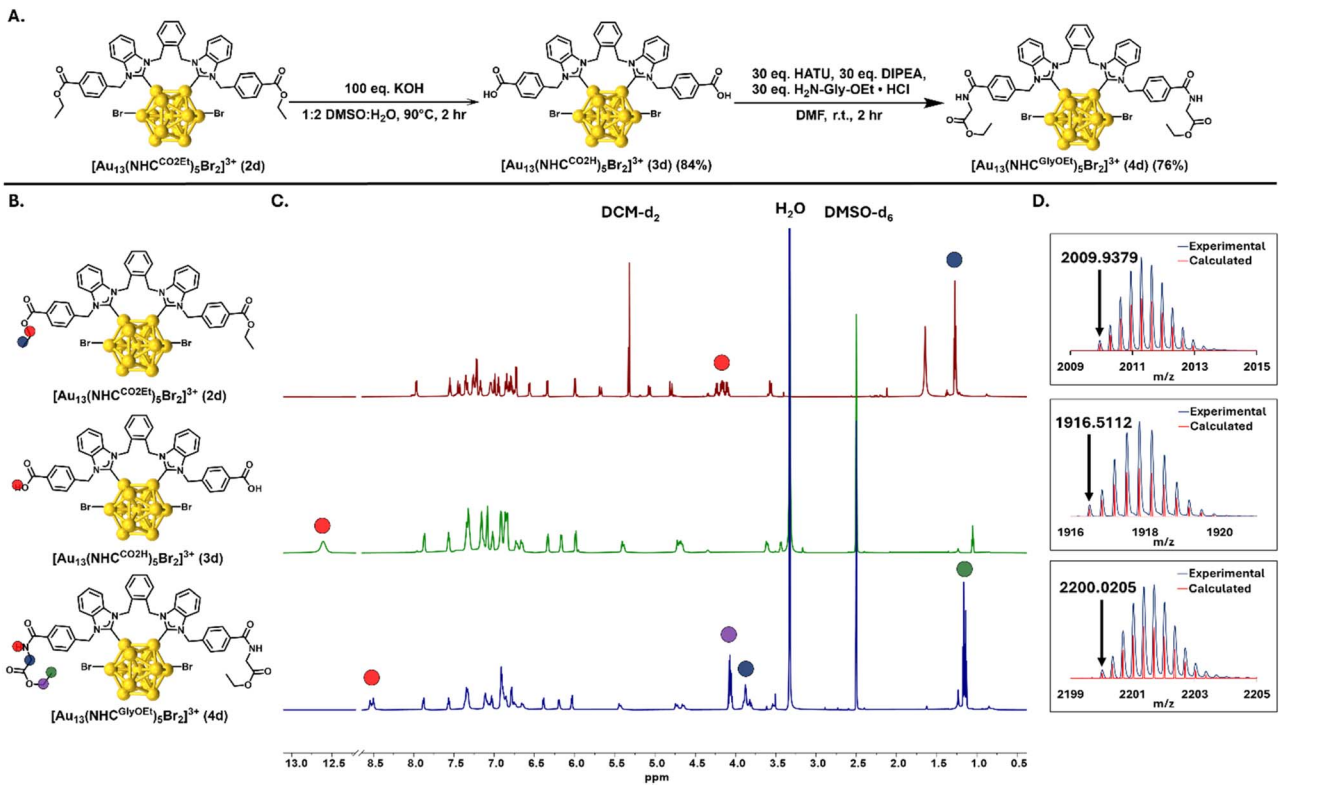

Fig. 2 (A) Synthesis of **3d** and **4d**. (B) Structures of **2d**, **3d**, and **4d**, highlighting key wingtip protons observable in ^{1}H NMR experiments. (C) ^{1}H NMR spectra of **2d** in DCM-d_2, and **3d** and **4d** in DMSO-d_6 depicting key signals on the wingtip groups. (D) ESI-MS spectra showing the experimental (blue) and calculated (red) isotope patterns of **2d**, **3d**, and **4d**.

diNHC cluster (**2c**) with the xylyl linked diNHC cluster (**2d**) reveals that the chelate effect is not the only factor contributing to the extremely high thermal stability of **2d**. Previous crystallographic evidence has shown there are CH–π and π–π interactions between the xylyl linker and the benzannulated NHC backbone of similar ditopic NHC-protected Au_{13} clusters.[38] These stabilizing interactions between the aromatic xylyl linker present in **2d** contribute to the higher stability than **2c**, preserving the Au_{13} core under the harsh saponification conditions necessary to achieve complete removal of the ethyl esters on the ligand shell. Thus, the successful saponification of cluster **2d** can be attributed to its high thermal stability under basic conditions rather than differences in reactivity of the ethyl ester groups between the other ester functionalized clusters **2a–c**.

Amide couplings on Au_{13}^{COOH} nanoclusters

To establish a method for tuning the biological properties of the prepared Au_{13}^{CO2H} nanoclusters (**3d**) *via* bioconjugation with amine-containing biomolecules, amide couplings were conducted with a simple C-terminally protected glycine residue using hexafluorophosphate azabenzotriazole tetramethyl uronium (HATU). Using the conditions described in Fig. 2A, 10 glycine ethyl ester residues were coupled to the surface of **3d** after 2 hours of reaction time as evidenced by the ESI-MS spectra depicting a single $[Au_{13}(NHC^{GlyOEt})_5Br_2]^{3+}$ peak at 2201 *m*/*z* (Fig. S12B). This produced a product that was insoluble in water, allowing the water-soluble starting materials to be removed with aqueous washes. Purification by column chromatography gave a fully coupled product in high yields (76%). ^{1}H NMR spectroscopy showed the disappearance of the broad singlet at 12.6 ppm from the –CO_2H functionality and the presence of new signals at 8.5 ppm (–N*H*), 4.1 ppm (–OCH_2), 3.8 ppm (–CH_2), and 1.1 ppm (–CH_3) attributed to the glycine residue, which integrated correctly to the protons on the rest of the NHC ligand (Fig. 2C). Interestingly, attempts at pre-activating the carboxylic acid with HATU and 1-ethyl-3-(3-dimethylaminopropyl)carbodiimide (EDC) followed by removal of the coupling reagents for subsequent coupling with glycine ethyl ester, in line with previously reported transformations with gold nanoparticles,[39] were unsuccessful.

To confirm that the ligand scaffold of **2d** had been preserved following saponification and amide coupling, ^{1}H, ^{13}C{^{1}H}, ^{1}H–^{1}H homonuclear correlation spectroscopy (COSY), and ^{1}H–^{13}C heteronuclear single quantum coherence (HSQC) experiments were conducted. The ^{1}H NMR spectra of **2d**, **3d**, and **4d** showed 8 unique CH_2 signals, identified by cross peaks with benzylic carbons in ^{1}H–^{13}C HSQC experiments (Fig. S38, S40, and S42). ^{1}H–^{1}H COSY experiments of these compounds revealed 4 pairs of CH_2 doublet signals which coupled to each other (Fig. S38, S40, and S42). These experiments show that the 4 benzylic CH_2 units on xylyl linked clusters are rigidly locked in unique chemical environments preventing free rotation of the hydrogen atoms and giving rise to 8 diastereotopic CH_2 doublet signals. ^{13}C{^{1}H} NMR spectra of **2d**, **3d**, and **4d** revealed that there are only two unique N*C*N chemical environments (Fig. S38, S40, and S42). These observations are consistent in the NMR spectra of **2a**, **3d**, and **4d**, suggesting each cluster has C_5 rotational symmetry with no horizontal plane of symmetry giving rise to a single ligand environment, which is preserved across all chemical transformations. These spectral observations are also consistent with Au_{13} clusters protected by similar ligand scaffolds suggesting that alterations to the wingtips of these clusters does not affect the conformation of the ligands.[38]

To evaluate the potential for bioconjugation of **3d** to peptides with potentially reactive side chains, we examined the coupling reaction with lysine residues protected with acid- and base-labile protecting groups commonly used in solid-phase peptide synthesis. Cluster **3d** was reacted with H-Lys(Boc)-O^{t}Bu using the same conditions described in Fig. 2A. ESI-MS confirmed that the completely coupled product was formed as the sole Au_{13} containing product (Fig. S13A). Furthermore, the acid-labile -Boc and -O^{t}Bu groups could be completely removed using 20% trifluoracetic acid (TFA) in DCM to produce a lysine functionalized cluster (**5d**) which was purified *via* SEC (see SI for details) to remove small molecular complex impurities and bulk gold species produced by significant aggregation of the cluster core during the harshly acidic deprotection (Fig. S13C). This synthesis was low yielding (20%) due to the instability of the cluster to harshly acidic conditions.

Next, a Lys(Fmoc)-OMe substrate was coupled to the cluster with ESI-MS confirming the formation of a single completely coupled product (Fig. S14A). Complete removal of the base labile -Fmoc and -OMe groups was achieved by stirring with 100 eq. LiOH in a 1 : 2 DMSO : H_2O solution for 2 hours to give **5d**. Following SEC (see SI for details), an improved 70% yield was obtained, indicating significantly improved stability under basic conditions (Fig. S14C). Due to the presence of basic –NH_2 and acidic –COOH functional groups, cluster **5d** was soluble in aqueous solutions at all pH values tested (pH = 1, 7, and 14).

These results demonstrate the robustness of this amide coupling procedure, allowing for the attachment of chemically diverse substrates and the removal of acid- and base-labile protecting groups. Consequently, this highly stable NHC framework can serve as a scaffold for the attachment of chemically diverse peptides to modulate the solubility and cellular uptake of the cluster.

Photoabsorption, photoluminescence and transient absorption properties

Optical absorbance profiles and emission maxima of clusters **2d**, **3d**, **4d**, and **5d** were measured to evaluate if post-synthetic modifications to the ligand shell changed the optical properties of the cluster (Fig. 3).[38] The characteristic spectral profiles of **2d**, **3d**, **4d**, and **5d** in the visible region, where metal-centered transitions occur,[37] closely resembled those of $[Au_{13}(diNHC)_5Cl_2]^{3+}$ having an icosahedral Au_{13} core.[38] The photoluminescence spectra of **2d**, **3d**, **4d**, and **5d** also remained unchanged following post-synthetic modifications to the ligand shell (Fig. 3). As such, post-synthetic modifications to the ligand shell have little effect on the geometric and electronic structures of the Au_{13} core, resulting in identical absorption and emission spectra in organic solvents.

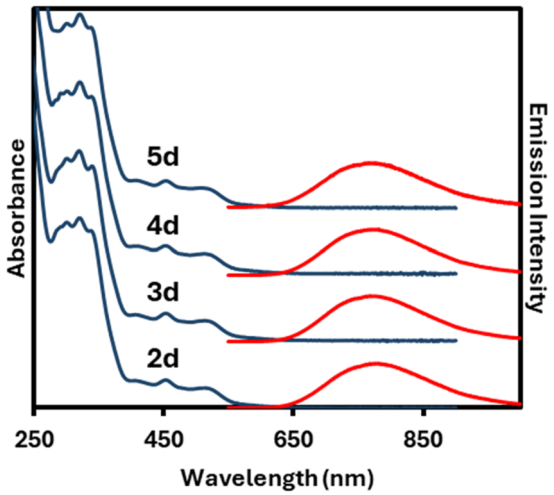

Fig. 3 UV-vis absorption spectra of clusters **2d**, **3d**, **4d**, and **5d** (blue) and their respective emission spectra excited at 453 nm (red). All spectra were taken in EtOH except for **5d** which was taken in MeOH due to solubility issue.

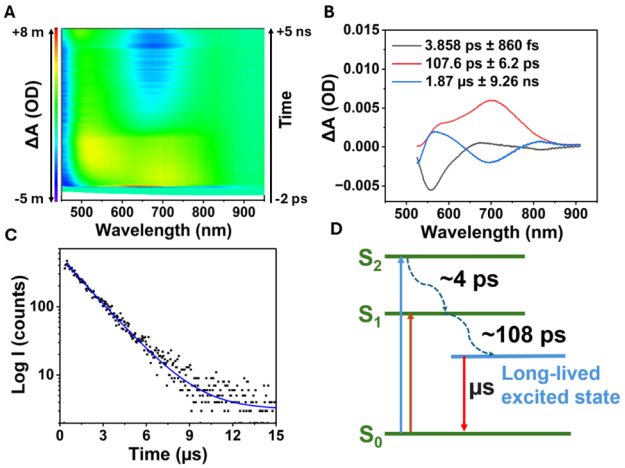

Fig. 4 (A) Femtosecond transient absorption spectrum of **3d** excited at 340 nm. (B) Three lifetime components simulated from global analysis that model the overall transient absorption spectrum. (C) Emission (775 nm) decay trace and fitting to a mono-exponential decay of **3d**. (D) Jablonski diagram of electronic excitation and excited state dynamics involved in the relaxation of **3d**.

The PLQYs (Φ_{PL}) of **2d**, **3d**, **4d**, and **5d** were determined by two methods (see SI for details) and are listed in Table 2. The Φ_{PL} remained high (~30%) for **2d**, **3d**, **4d**, and **5d** in organic solvents indicating that the NHC framework surrounding the Au_{13} core remains rigid despite the addition of larger, more flexible species to the wingtips, thus preventing non-radiative decay *via* vibrational relaxation. This allows for the surface chemistry of the cluster to be tuned independently of the core structure which has a greater influence on the photoabsorption and photoluminescence properties.

In PBS solutions, the λ_{PL} of **3d** and **5d** were red-shifted, which may indicate the stabilization of the emissive photoexcited state in water. The Φ_{PL} of **3d** in PBS was also significantly improved upon conjugation to lysine (**5d**). The $-CO_2H$ and $-NH_2$ functionalities in **3d** and **5d** can lead to pH-dependent charge states of the ligand shell, which can affect the electronic structure of the cluster.[40]

In contrast, changing the ancillary NHC ligand system to monotopic substituents led to a blue shift of the emission maximum (**2a**: 695 nm in MeOH; **2b**: 775 nm). Whereas the imidazole-protected cluster **2a** displayed a high Φ_{PL} of 17% in MeOH, the respective benzimidazole-protected cluster showed a notably reduced PL quantum yield (Φ_{PL}) of 3% in EtOH. As apparent from cluster **2c**, the linker unit of ditopic NHC–Au clusters affects the PL properties of clusters to a larger degree than changes to the NHC wingtip. Relative to cluster **2d**, bridged by a *o*-xylyl linker, the λ_{PL} of **2c** (755 nm in MeOH) bridged by a propyl linker is blue-shifted by 25 nm. Likewise, a lower Φ_{PL} of 12% was observed, which is likely caused by a reduced ability of the propyl-linked NHC to rigidify the cluster core, leading to a promotion of non-radiative quenching of the excited state.

To further investigate the excited state properties and reactivity of cluster **3d**, transient absorption and photoluminescence lifetime studies were undertaken in MeOH. Fig. 4 shows a transient absorption spectrum for **3d** and corresponding Jablonski diagram illustrating the observed relaxation pathways for cluster **3d**. Importantly, this cluster exhibits a long lived, 1.9 μs excited state, responsible for the emission properties of the cluster. The time scale is consistent with phosphorescent emission, but further experiments are needed to conclude intersystem crossing and the involvement of the triplet excited state. This long-lived excited state may prove advantageous for reacting with oxygen or other intracellular species for cancer therapy.

Table 2 PL emission maxima and quantum yields[a]

Cluster	λ_{PL} (nm)	Relative Φ_{PL} (%)	Absolute Φ_{PL} (%)
2d (EtOH)	780	32	31
3d (EtOH)	780	31	30
3d (PBS)	828	6	4
4d (EtOH)	780	30	29
5d (MeOH)	780	28	25
5d (PBS)	797	12	9

[a] Methods for determination of QY are given in the SI.

Biostability studies

Finally, we studied the stability of water-soluble clusters **3d** and **5d** in phosphate buffered saline (PBS) solution and in PBS with added glutathione (GSH, 2 mM) at 37 °C (Fig. S1). Both clusters **3d** and **5d** were stable for 24 hours at 37 °C in PBS solution, showing minimal changes to their UV-vis absorption profiles (Fig. S1). Cluster **3d** was further studied under various physiologically relevant conditions and with rigorous emission spectroscopic analysis (Fig. S1–S5), confirming the good stability of these clusters under the conditions noted. In PBS solutions with 2 mM GSH at 37 °C, clusters **3d** and **5d** decomposed

significantly over 24 h as evidenced by the near complete loss of characteristic absorption bands in the visible region. ESI-MS of cluster **3d** following 24 hours of exposure to 2 mM GSH revealed the presence of an $[Au_{13}(NHC^{COOH})_5(Br)(GS)]^{3+}$ ion as a minor species indicating that the cluster was slowly undergoing ligand exchange of the halides with the excess glutathione in solution (Fig. S6). However, an $[Au_{13}(NHC^{Lys})_5(Br)(GS)]^{3+}$ ion could not be observed for **5d**, although GS incorporation at the halide position is also possible. Consequently, bioconjugation of the cluster to longer amino acid chains and other larger biomolecules is a good possible route to tuning biocompatibility while maintaining cluster stability. It is also important to note that the NHC ligands remain ligated and the cluster core remains intact under these conditions and that high stability in the case of the parent cluster **3d** is observed in the absence of glutathione, which is likely related to the strong NHC–Au bonds.

Conclusion

In conclusion, we have described the synthesis of a highly stable and water-soluble carboxylate-functionalized $[Au_{13}(NHC^{COOH})_5Br_2]Br_3$ cluster (**3a**) that is stable under a wide range of conditions needed for bio-conjugation. Amide coupling reactions on **3a** allowed the solubility and surface chemistry of the cluster to be tuned with simple and accessible amine coupling partners. This cluster was shown to be resistant to degradation and structural rearrangement at high temperatures (90 °C) and at pH extremes. NMR spectroscopic and optical analyses indicate that the rigid NHC scaffold and highly stable superatomic Au_{13} core were preserved following several post-synthetic modifications to the wingtips of the NHC ligands. Photoluminescence properties and stability were observed to be highly dependent on the denticity of the NHC ligand, benzannulation of the NHC ligand, and the nature of the linking group between diNHC ligands. Post-synthetic modifications to the wingtips of NHC ligands on stable clusters were observed to induce minimal changes to the photoabsorption and photoluminescence properties of the cluster in organic solvents.

This study is one of the first examples detailing how the biological properties of AuNCs, which are primarily dictated by their hydrodynamic size and their organic ligands,[41] can be tuned independently of their photoabsorption and photoluminescence properties. We envisage that the development of methods for the post-synthetic functionalization of AuNCs will enable their pharmacokinetics and pharmacodynamics to be altered similarly to small molecule therapeutics, accelerating the use of AuNCs in a therapeutic setting.

Author contributions

ALDML, DAB, CMC, TT and ST conceptualized the project. ALDML conducted laboratory experiments and curated the data on **2d**, **3d**, **4d**, and **5d**. DAB conducted laboratory experiments and curated the data on **2a–c**. PA conducted transient absorption studies, lifetime measurements, stability studies and interpretted the data, along with KS. AIS assisted with laboratory experiments and data collection. ALDML, DAB and PA wrote the original draft. All authors were responsible for reviewing and editing the draft. Single-crystal X-ray diffraction analyses and crystal structure refinement were conducted by DAB and ST. CMC, TT, and KS provided funding for the project.

Conflicts of interest

There are no conflicts to declare.

Data availability

The data supporting this article have been included as part of the SI. Crystallographic data for 1,3-bis(benzimidazolyl) propane, **1c**, **1d**, and **2a**$[PF_6]_2$ has been deposited at CCDC under 2444794, 2444795, 2444796, and 2444843.

Supplementary crystallographic data for this paper can be obtained free of charge *via* the joint Cambridge Crystallographic Data Centre (CCDC) and Fachinformationszentrum Karlsruhe Access Structures service.

Supplementary information is available includes full characterization data for clusters including NMR spectra, photophysical characterization and stability studies. See DOI: **https://doi.org/10.1039/d5sc02951a**.

Acknowledgements

This work was carried out with the support of the Carbon to Metal Coating Institute at Queen's University and the New Foundations in Research Fund-Transformation (NFRF-T) program (#NFRFT-2020-00573). The Natural Sciences and Engineering Research Council of Canada (NSERC), the Social Sciences and Humanities Research Council (SSHRC), the Canada Foundation for Innovation (CFI) and the Canada Research Chairs Program are thanked for financial support of this work in terms of operating, equipment and Chair support to CMC. Queen's University is thanked for general support and for a Distinguished University Professorship to C. M. C. JSPS and NU are acknowledged for funding of this research through The World Premier International Research Center Initiative (WPI) program. T. T. thanks JST, CREST (Grant No. JPMJCR20B2) for financial support. C. M. C. thanks the Canada Research Chairs Program for support. A. D. L. M. L. thanks the NSERC-CREATE Materials for Advanced Photonics and Sensing (MAPS) program and the Government of Ontario for scholarship support.

Notes and references

1 X.-D. Zhang, D. Wu, X. Shen, P.-X. Liu, F.-Y. Fan and S.-J. Fan, In vivo renal clearance, biodistribution, toxicity of gold nanoclusters, *Biomaterials*, 2012, **33**(18), 4628–4638, DOI: **10.1016/j.biomaterials.2012.03.020**.

2 H. Cui, Z.-S. Shao, Z. Song, Y.-B. Wang and H.-S. Wang, Development of gold nanoclusters: from preparation to applications in the field of biomedicine, *J. Mater. Chem. C*, 2020, **8**(41), 14312–14333, DOI: **10.1039/D0TC03443F**.

3 H. Li, H. Li and A. Wan, Luminescent gold nanoclusters for in vivo tumor imaging, *Analyst*, 2020, **145**(2), 348–363, DOI: 10.1039/C9AN01598A.
4 S. Zhu, X. Wang, Y. Cong and L. Li, Regulating the Optical Properties of Gold Nanoclusters for Biological Applications, *ACS Omega*, 2020, **5**(36), 22702–22707, DOI: 10.1021/acsomega.0c03218.
5 Z. Liu, L. Luo and R. Jin, Visible to NIR-II Photoluminescence of Atomically Precise Gold Nanoclusters, *Adv. Mater.*, 2024, **36**(8), 2309073, DOI: 10.1002/adma.202309073.
6 X. Qu, Y. Li, L. Li, Y. Wang, J. Liang and J. Liang, Fluorescent Gold Nanoclusters: Synthesis and Recent Biological Application, *J. Nanomater.*, 2015, **2015**(1), 784097, DOI: 10.1155/2015/784097.
7 H. Liu, L. Wang, Z. Xue and X.-D. Zhang, Atomic Precise Gold Nanoclusters: Toward the Customize Synthesis, Precision Medicine, *Part. Part. Syst. Charact.*, 2023, **40**(9), 2300084, DOI: 10.1002/ppsc.202300084.
8 R. Jin, Atomically precise metal nanoclusters: stable sizes and optical properties, *Nanoscale*, 2015, **7**(5), 1549–1565, DOI: 10.1039/C4NR05794E.
9 W. Jiang, B. Y. S. Kim, J. T. Rutka and W. C. W. Chan, Nanoparticle-mediated cellular response is size-dependent, *Nat. Nanotechnol.*, 2008, **3**(3), 145–150, DOI: 10.1038/nnano.2008.30.
10 W. Kurashige, Y. Niihori, S. Sharma and Y. Negishi, Precise synthesis, functionalization and application of thiolate-protected gold clusters, *Coord. Chem. Rev.*, 2016, **320–321**, 238–250, DOI: 10.1016/j.ccr.2016.02.013.
11 Z. Lei, X. K. Wan, S. F. Yuan, Z. J. Guan and Q. M. Wang, Alkynyl Approach toward the Protection of Metal Nanoclusters, *Acc. Chem. Res.*, 2018, **51**(10), 2465–2474, DOI: 10.1021/acs.accounts.8b00359.
12 M.-M. Zhang, X.-Y. Dong, Y.-J. Wang, S.-Q. Zang and T. C. W. Mak, Recent progress in functional atom-precise coinage metal clusters protected by alkynyl ligands, *Coord. Chem. Rev.*, 2022, **453**, 214315, DOI: 10.1016/j.ccr.2021.214315.
13 R. H. Adnan, J. M. L. Madridejos, A. S. Alotabi, G. F. Metha and G. G. Andersson, A Review of State of the Art in Phosphine Ligated Gold Clusters and Application in Catalysis, *Advanced Science*, 2022, **9**(15), 2105692, DOI: 10.1002/advs.202105692.
14 H. Shen, G. Tian, Z. Xu, L. Wang, Q. Wu, Y. Zhang, B. K. Teo and N. Zheng, N-heterocyclic carbene coordinated metal nanoparticles and nanoclusters, *Coord. Chem. Rev.*, 2022, **458**, 214425, DOI: 10.1016/j.ccr.2022.214425.
15 E. L. Albright, T. I. Levchenko, V. K. Kulkarni, A. I. Sullivan, J. F. DeJesus, S. Malola, S. Takano, M. Nambo, K. Stamplecoskie, H. Häkkinen, T. Tsukuda and C. M. Crudden, N-Heterocyclic Carbene-Stabilized Atomically Precise Metal Nanoclusters, *J. Am. Chem. Soc.*, 2024, **146**(9), 5759–5780, DOI: 10.1021/jacs.3c11031.
16 D. A. Buschmann, H. Hirai and T. Tsukuda, Tuning photoluminescence properties of Au clusters by surface modification and doping: lessons from case studies of icosahedral Au_{13}, *Inorg. Chem. Front.*, 2024, **11**, 6694–6710, DOI: 10.1039/D4QI01773K.
17 X.-L. Pei, P. Zhao, H. Ube, Z. Lei, K. Nagata, M. Ehara and M. Shionoya, Asymmetric Twisting of C-Centered Octahedral Gold(I) Clusters by Chiral N-Heterocyclic Carbene Ligation, *J. Am. Chem. Soc.*, 2022, **144**(5), 2156–2163, DOI: 10.1021/jacs.1c10450.
18 T. Higaki, Q. Li, M. Zhou, S. Zhao, Y. Li, S. Li and R. Jin, Toward the Tailoring Chemistry of Metal Nanoclusters for Enhancing Functionalities, *Acc. Chem. Res.*, 2018, **51**(11), 2764–2773, DOI: 10.1021/acs.accounts.8b00383.
19 T. Tsukuda, Toward an Atomic-Level Understanding of Size-Specific Properties of Protected and Stabilized Gold Clusters, *Bull. Chem. Soc. Jpn.*, 2012, **85**(2), 151–168, DOI: 10.1246/bcsj.20110227.
20 A. I. Sullivan, E. A. Steele, S. Takano, E. Zeinizade, J. Chen, S. Malola, K. Siddhant, H. Häkkinen, K. G. Stamplecoskie, T. Tsukuda, G. Zheng and C. M. Crudden, Diving into Unknown Waters: Water-Soluble Clickable Au_{13} Nanoclusters Protected with N-Heterocyclic Carbenes for Bio-Medical Applications, *J. Am. Chem. Soc.*, 2025, **147**(5), 4230–4238, DOI: 10.1021/jacs.4c14240.
21 J. F. DeJesus, S. I. Jacob, Q. M. Phung, K. Mimura, Y. Aramaki, T. Ooi, M. Nambo and C. M. Crudden, If the Crown Fits: Sterically Demanding N-Heterocyclic Carbene Promotes the Formation of Au_8Pt Nanoclusters, *J. Am. Chem. Soc.*, 2024, **146**(34), 23806–23813, DOI: 10.1021/jacs.4c04873.
22 V. K. Kulkarni, E. L. Albright, E. Zeinizade, E. Steele, J. Chen, L. Ding, S. Malola, S. Takano, K. Harrington, N. Kwon, *et al.*, Impact of Ligand Structure on Biological Activity and Photophysical Properties of NHC-Protected Au_{13} Nanoclusters, *J. Am. Chem. Soc.*, 2025, **147**(5), 4017–4025, DOI: 10.1021/jacs.4c12072.
23 X.-R. Song, N. Goswami, H.-H. Yang and J. Xie, Functionalization of metal nanoclusters for biomedical applications, *Analyst*, 2016, **141**(11), 3126–3140, DOI: 10.1039/C6AN00773B.
24 Y. Zheng, L. Lai, W. Liu, H. Jiang and X. Wang, Recent advances in biomedical applications of fluorescent gold nanoclusters, *Adv. Colloid Interface Sci.*, 2017, **242**, 1–16, DOI: 10.1016/j.cis.2017.02.005.
25 P. N. Gunawardene, J. F. Corrigan and M. S. Workentin, Golden Opportunity: A Clickable Azide-Functionalized $[Au_{25}(SR)_{18}]^-$ Nanocluster Platform for Interfacial Surface Modifications, *J. Am. Chem. Soc.*, 2019, **141**(30), 11781–11785, DOI: 10.1021/jacs.9b05182.
26 Y. Zhang, S.-R. He, Y. Yang, T.-S. Zhang, Z.-M. Zhu, W. Fei and M.-B. Li, Preorganized Nitrogen Sites for Au_{11} Amidation: A Generalizable Strategy toward Precision Functionalization of Metal Nanoclusters, *J. Am. Chem. Soc.*, 2023, **145**(22), 12164–12172, DOI: 10.1021/jacs.3c01961.
27 K. Pyo, H. Xu, S. M. Han, S. Saxena, S. Y. Yoon, G. Wiederrecht, G. Ramakrishna and D. Lee, Synthesis and Photophysical Properties of Light-Harvesting Gold Nanoclusters Fully Functionalized with Antenna

Chromophores, *Small*, 2021, **17**(27), 2004836, DOI: **10.1002/smll.202004836**.

28 E. Oh, F. K. Fatemi, M. Currie, J. B. Delehanty, T. Pons, A. Fragola, S. Lévêque-Fort, R. Goswami, K. Susumu, A. L. Huston, *et al.*, PEGylated Luminescent Gold Nanoclusters: Synthesis, Characterization, Bioconjugation, and Application to One- and Two-Photon Cellular Imaging, *Part. Part. Syst. Charact.*, 2013, **30**(5), 453–466, DOI: **10.1002/ppsc.201200140**.

29 Z. Liu, L. Turyanska, F. Zamberlan, S. Pacifico, T. D. Bradshaw, F. Moro, M. W. Fay, H. E. L. Williams and N. R. Thomas, Synthesis of folic acid functionalized gold nanoclusters for targeting folate receptor-positive cells, *Nanotechnology*, 2019, **30**, 505102, DOI: **10.1088/1361-6528/ab437c**.

30 X. Liu, X. Hou, Z. Li, J. Li, X. Ran and L. Yang, Water-soluble amino pillar[5]arene functionalized gold nanoclusters as fluorescence probes for the sensitive determination of dopamine, *Microchem. J.*, 2019, **150**, 104084, DOI: **10.1016/j.microc.2019.104084**.

31 K. J. Malawska, S. Takano, K. Oisaki, H. Yanagisawa, M. Kikkawa, T. Tsukuda and M. Kanai, Bioconjugation of Au_{25} Nanocluster to Monoclonal Antibody at Tryptophan, *Bioconjugate Chem.*, 2023, **34**(4), 781–788, DOI: **10.1021/acs.bioconjchem.3c00069**.

32 X. Jiang, B. Du, Y. Huang, M. Yu and J. Zheng, Cancer Photothermal Therapy with ICG-Conjugated Gold Nanoclusters, *Bioconjugate Chem.*, 2020, **31**(5), 1522–1528, DOI: **10.1021/acs.bioconjchem.0c00172**.

33 C. Zeng, Y. Chen, A. Das and R. Jin, Transformation Chemistry of Gold Nanoclusters: From One Stable Size to Another, *J. Phys. Chem. Lett.*, 2015, **6**(15), 2976–2986, DOI: **10.1021/acs.jpclett.5b01150**.

34 Y. Li, H. Cheng, T. Yao, Z. Sun, W. Yan, Y. Jiang, Y. Xie, Y. Sun, Y. Huang, S. Liu, *et al.*, Hexane-Driven Icosahedral to Cuboctahedral Structure Transformation of Gold Nanoclusters, *J. Am. Chem. Soc.*, 2012, **134**(43), 17997–18003, DOI: **10.1021/ja306923a**.

35 R. Jin, H. Qian, Z. Wu, Y. Zhu, M. Zhu, A. Mohanty and N. Garg, Size Focusing: A Methodology for Synthesizing Atomically Precise Gold Nanoclusters, *J. Phys. Chem. Lett.*, 2010, **1**(19), 2903–2910, DOI: **10.1021/jz100944k**.

36 J. Liu, Y. Sato, V. K. Kulkarni, A. I. Sullivan, W. Zhang, C. M. Crudden and J. E. Hein, Insights into the synthesis of NHC-stabilized Au nanoclusters through real-time reaction monitoring, *Chem. Sci.*, 2023, **14**(38), 10500–10507, DOI: **10.1039/D3SC02077K**.

37 M. R. Narouz, S. Takano, P. A. Lummis, T. I. Levchenko, A. Nazemi, S. Kaappa, S. Malola, G. Yousefalizadeh, L. A. Calhoun, K. G. Stamplecoskie, *et al.*, Robust, Highly Luminescent Au_{13} Superatoms Protected by N-Heterocyclic Carbenes, *J. Am. Chem. Soc.*, 2019, **141**(38), 14997–15002, DOI: **10.1021/jacs.9b07854**.

38 H. Yi, K. M. Osten, T. I. Levchenko, A. J. Veinot, Y. Aramaki, T. Ooi, M. Nambo and C. M. Crudden, Synthesis and enantioseparation of chiral Au_{13} nanoclusters protected by bis-N-heterocyclic carbene ligands, *Chem. Sci.*, 2021, **12**(31), 10436–10440, DOI: **10.1039/D1SC03076K**.

39 L. C. Ekowo, N. L. Dominique, G. Kaur, D. M. Jenkins and J. P. Camden, Using LDI-MS to Explore Amide Coupling Reactions with Carboxylate Terminated N-Heterocyclic Carbene Monolayers, *J. Am. Soc. Mass Spectrom.*, 2025, **36**(5), 1182–1190, DOI: **10.1021/jasms.5c00047**.

40 S. Zhou, L. Gustavsson, G. Beaune, S. Chandra, J. Niskanen, J. Ruokolainen, J. V. I. Timonen, O. Ikkala, B. Peng and R. H. A. Ras, pH-Responsive Near-Infrared Emitting Gold Nanoclusters, *Angew. Chem., Int. Ed.*, 2023, **62**(49), e202312679, DOI: **10.1002/anie.202312679**.

41 Y. Genji Srinivasulu, Q. Yao, N. Goswami and J. Xie, Interfacial engineering of gold nanoclusters for biomedical applications, *Mater. Horiz.*, 2020, **7**(10), 2596–2618, DOI: **10.1039/D0MH00827C**.